Raman Spectra Variation of Partially Suspended Individual Single-Walled Carbon Nanotubes

Yingying Zhang,[†] Hyungbin Son,[‡] Jin Zhang,*[,†] Mildred S. Dresselhaus,[‡,§] Jing Kong,*[,‡] and Zhongfan Liu*[,†]

Centre for Nanoscale Science and Technology (CNST), Beijing National Laboratory for Molecular Sciences (BNLMS), State Key Laboratory for Structural Chemistry of Unstable and Stable Species, Key Laboratory for the Physics and Chemistry of Nanodevices, College of Chemistry and Molecular Engineering, Peking University, Beijing 100871, P.R. China, and Department of Electrical Engineering and Computer Science and Department of Physics, Massachusetts Institute of Technology, Cambridge, Massachusetts 02139

Received: September 13, 2006; In Final Form: October 30, 2006

The electrical and optical properties of single-walled carbon nanotubes (SWNTs) have been shown to be sensitive to their environment. Therefore it is very important to understand and exploit the environmental effect on the properties of nanotubes, especially for individual SWNTs. We report herein a systematic investigation of the Raman spectra variation of 15 individual SWNTs partially suspended on trench-contained substrates. Our experiments are conducted with low laser power to exclude possible heating effects. Most SWNTs show enhanced Raman signals for their suspended segment compared with their segment sitting on the SiO_2 substrate, with several exceptions exhibiting either similar Raman intensity or a reverse result. Apart from this distinct intensity contrast, moderate radial breathing mode (RBM) frequency variations are observed for some nanotubes, which can be attributed to nanotube−substrate interactions. By analyzing the behaviors of the RBM full width at half-maximum (fwhm) and the intensity ratio between the anti-Stokes and Stokes spectra (I_{AS}/I_S), we can infer the shift of the nanotube transition energy E_{ii} for the segment of nanotube sitting on the substrate relative to the freely suspended segment. These Raman spectra variations can be attributed to the van der Waals interactions between the nanotube and the substrate, which give rise to both a structural modification (as a radial deformation) and an electronic modification (as a change in the electronic density of states) for the nanotubes on substrate.

Introduction

Resonance Raman spectroscopy has been demonstrated to provide a powerful tool for characterizing the structure of carbon nanotubes (CNTs). In particular, a strong Raman signal can be observed for an individual single-walled carbon nanotube (SWNT), when one of its electronic transition energies E_{ii} is in resonance with the laser energy E_{laser}. By comparing the experimental resonant energy E_{ii} and the radial breathing mode (RBM) frequency ω_{RBM} with the theoretically calculated Kataura plot, it is possible to determine the diameter and the chiral indicies (n,m) of the SWNT.[1]

The Raman spectra of SWNTs have been shown to be sensitive to the nanotube's environment,[2−4] including whether the tube is in a bundle or is an isolated SWNT, or whether it is in a solution or sitting on a substrate or freely suspended. For nanotube samples in solution, the wrapping agents and solvents represent different environments as well, since they can be polar or nonpolar. Since the ω_{RBM} is of great importance for deducing the geometric structure of a SWNT by resonance Raman spectroscopy and E_{ii} is an essential factor determining the electrical and optical properties of the SWNT, it is very important to understand and exploit these environmental effects.[5−8] Theoretical calculations have predicted that tube−tube interactions within a bundle will cause a ∼6−20 cm^{-1} upshift in RBM frequencies compared with isolated tubes due to the space restrictions imposed by the presence of neighboring tubes.[9−11] It was also inferred from experiments that the resonant energy E_{ii} of a SWNT in a bundle will be higher than when the nanotube is isolated.[12] However, more recent studies show an unchanged ω_{RBM} frequency but lower E_{ii} for nanotubes in bundles compared with isolated tubes wrapped by sodium dodecyl sulfate (SDS) in aqueous solution.[2] These previous investigations were all carried out with SWNT samples in bulk form, either as a solid or dispersed in solution. A direct investigation on specific individual SWNTs will be highly desirable to uncover and clarify further details regarding environmental effects. Such studies are lacking at present.

In our recent communication,[13] ultralong individual SWNTs were successfully prepared on trench-containing substrates, which provide nanotubes with both suspended and nonsuspended segments. These samples serve as ideal systems for investigating environmental effects (in this case, substrate interactions) on individual SWNTs. In the present work, we report on the Raman signal variation (in terms of the intensity, frequency, line width, and intensity ratio between Stokes and anti-Stokes signals) by comparing the corresponding Raman features between the suspended and nonsuspended segments along the same SWNT. Our experiments are carried out with low enough laser excitation power so that the effect of laser heating on the suspended segments can be excluded. We collected RBM and G-mode Raman spectra for 15 individual SWNTs and compared the

[†] Peking University.
[‡] Department of Electrical Engineering and Computer Science, Massachusetts Institute of Technology.
[§] Department of Physics, Massachusetts Institute of Technology.

10.1021/jp065973l CCC: $37.00
Published on Web 01/11/2007

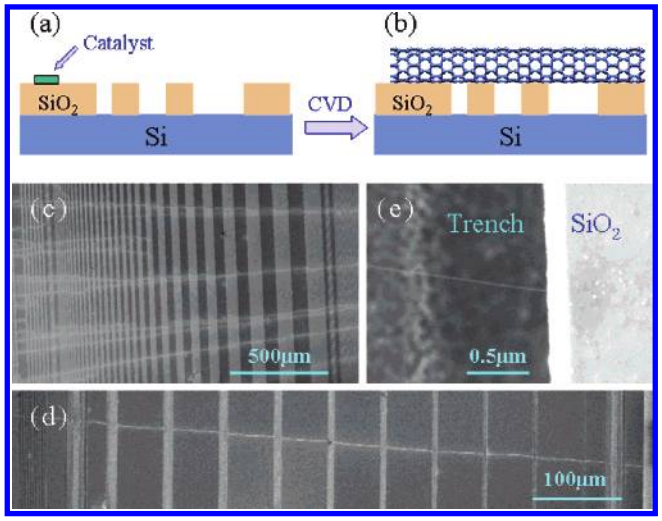

Figure 1. (a) A schematic illustration of the trench-containing substrate (type A) with the catalyst being deposited at one edge of the substrate and used for the subsequent CVD preparation of SWNTs. (b) A schematic illustration of an individual SWNT suspended over trenches. (c) An SEM image showing oriented long SWNTs on a trench (300 nm deep)-containing substrate. (d) An SEM image of an individual SWNT crossing trenches (10 nm deep, 1 to 10 μm wide). (e) A zoom-in SEM image at one edge of a trench (10 μm deep, 6 μm wide) showing that the nanotube is well suspended over the trench. (In the SEM image, the lighter color indicates the trench.)

observed variations in detail, and the environment effects on the same nanotube have been systematically studied.

Experimental Section

A. SWNT Preparation and Characterization. An illustration of the sample preparation is shown in Figure 1, parts a and b. The substrates used in this study are silicon pieces with a 300 nm thick SiO_2 film. Photolithography and dry etching were used to pattern 1−80 μm wide trenches on the surface. Two types of substrates with trench depths of 300 nm (type A) and 10 μm (type B) were used in this study.

SWNTs were grown by the catalytic chemical vapor decomposition (CVD) of ethanol.[14] A 0.01 M $FeCl_3$ ethanol solution was applied by microcontact printing to one edge of the substrate. The substrate was then placed in a horizontal 1.5 in. quartz furnace with the catalyst end directed toward the gas flow. The substrate was heated at 900 °C for 30 min in a flow of Ar/H_2 (500 sccm/30 sccm) and then ethanol was introduced into the furnace by bubbling 200 sccm Ar through the ethanol. The growth was terminated after 30 min by switching the gas to Ar/H_2 (500 sccm/30 sccm) and cooling the furnace.

As shown in Figure 1c, an SEM image of the prepared samples revealed that well-separated, millimeter to centimeter long carbon nanotubes with a controlled orientation can be routinely prepared on the trench-containing substrate. For the samples with 300 nm deep trenches, carbon nanotubes can be suspended over 3 μm wide trenches, while for the sample with 10 μm deep trenches, nanotubes are suspended over 10 μm wide trenches. For wider trenches, some SWNTs come into contact with the bottom of the trench. Parts d and e of Figure 1 show an individual SWNT that spans the trenches with 1 to 10 μm widths and is well suspended over them. This indicates that the nanotubes are floating above the substrate during the growth.

B. Raman Spectra Measurements. Resonant Raman spectroscopy (Renishaw microprobe RM1000) with a 632.8 nm (1.96 eV) He−Ne laser was used in this study. The excitation spot size is about 1 μm^2, using a 50× objective lens. The excitation laser power ranges from 0.04 to 1.07 mW at the sample. With the help of the SEM image and using the trench structures on the substrate as markers, a micro-Raman spectroscopy study on an individual nanotube can be readily carried out. Generally, we first scan the laser spot along a trench (which is perpendicular to the SWNTs) to find resonant nanotubes. We next locate the precise position of a particular SWNT by looking for the strongest signal to make sure that the laser spot is right on top of the nanotube, and then we collect Raman spectra at that location. All spectra are taken with the light polarized parallel along the nanotube axis. Raman spectra of the 15 SWNTs (12 are on the type A substrate and 3 are on the type B substrate, see Table 1) are obtained from both the suspended (SUS) segments and the sitting-on-substrate (SOS) segments. The signals of the suspended segment of the 12 nanotubes on the type A substrate are taken over the 3 μm wide trenches, those of the No. 6 and No. 13 nanotubes are taken from the 6 μm wide trenches, those of the No. 14 nanotubes are taken from a 4 μm wide trench. In fact, our intention of using the type B substrate (deeper trenches, and nanotubes can be suspended over wider trenches) is to check whether the signals of the suspended segment of the same nanotube are the same over trenches with different widths. As observed experimentally, the Raman behaviors of suspended SWNTs are the same as long as the distance between the laser spot and the trench edge is above 1.5 μm (including 1.5 μm). So, as the signals for the suspended segments of these 15 SWNTs are all taken from trenches with width ≥3 μm (2 × 1.5 μm), it is reasonable to put them together for comparison. We focus on the RBM and G-band features in this study. The RBM peak positions (ω_{RBM}), intensity, and full width at half-maximum (fwhm) are all obtained by fitting the spectra with use of a Lorentzian line shape. These values as well as the change in RBM frequency ($\Delta\omega_{RBM}$) and the anti-Stokes to Stokes RBM intensity ratios (I_{AS}/I_S) between the two segments are summarized in Table 1.

TABLE 1: Summary of Data for 15 SWNTs That Were Investigated in This Study, among Which Three SWNTs (Nos. 6, 13, and 14) are on a Type B Substrate (10 μm Deep Trench) and the Others are on a Type A (300 nm Deep Trench) Substrate[a]

	ω_{RBM} (cm^{-1})		fwhm (cm^{-1})		I_{AS}/I_S		RBM intensity	
no.	SUS	$\Delta\omega_{RBM}$	SUS	SOS	SUS	SOS	SU) (au)	I_{SUS}/I_{SOS}
1	282.5	0	2.4	2.8	0.12	0.09	0.038	2.3
2	243.7	+1.3	5.6	3.8	1.23	0.88	0.0088	0.53
3	201.7	0	7.0	7.0	0.10	0.16	0.11	2.4
4	200.4	−0.1	3.6	4.8	0.13	0.14	0.0078	0.087
5	193.7	+0.6	4.4	5.3	0.14	0.16	1.0	18
6	187.4	+0.9	2.9	2.7	0.13	0.18	0.061	0.94
7	169.8	−0.3	2.8	2.8	0.40	0.27	0.39	4.1
8	167.6	0	3.1	3.3	0.80	0.80	0.0095	2.5
9	159.9	0	4.0	6.4	1.0	0.70	0.0050	1.1
10	157.5	−0.8	8.2	13	0.96	0.39	0.0067	2.2
11	148.4	−0.3	3.6	4.5	1.1	0.60	0.038	2.6
12	144.0	+0.6	4.1	4.0	0.82	0.84	0.0063	5.4
13	129.9	0	5.4	11	1.7	0.44	0.0073	3.2
14	117.0	0	4.9	4.0	0.7	1.20	0.017	14
15	115.8	−0.3	4.6	7.1	1.55	1.25	0.048	30

[a] Each row corresponds to data taken from the same SWNT. SUS indicates the data of a suspended segment and SOS means that from a segment sitting on a substrate. I_{AS}/I_S is the intensity ratio of the anti-Stokes to Stokes of the RBM features and fwhm (cm^{-1}) is the full width at half-maximum of the RBM Raman peak. The units of the intensity are arbitrary and in this table we use the highest intensity as a normalization factor. I_{SUS}/I_{SOS} is the intensity ratio of the SUS segment to the SOS segment of the same SWNT.

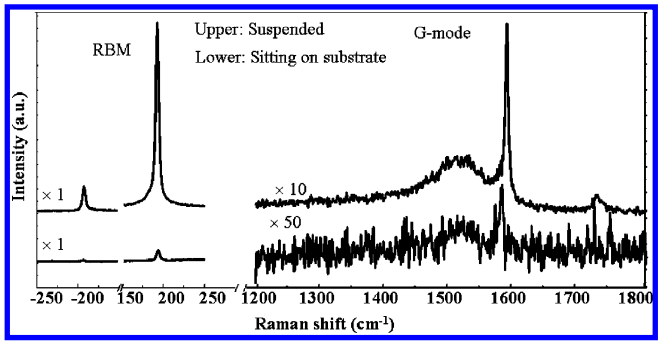

Figure 2. Raman spectra from a suspended segment (upper line) and from a segment sitting on substrate (lower line) of an individual SWNT. All the spectra are collected with a laser power of 0.13 mW and the integration time is 30 s. The G mode intensity is multiplied by 10 (suspended) and by 50 (sitting on substrate) to display the spectra clearly in the same panel of the figure.

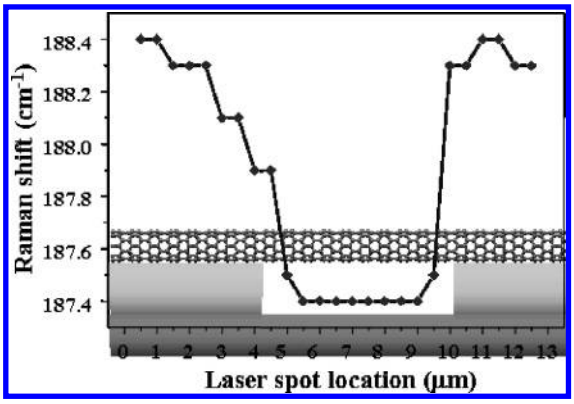

Figure 3. RBM frequency variation of an individual SWNT (No. 6) with the laser spot moving along the tube (0.5 μm per step) from the left side to the right side of a 6 μm wide trench. The laser power level used here is 0.31 mW. A schematic illustration of the trench-containing substrate is included on the bottom to show the laser spot location.

Note that, although the resolution of the spectrometer is about $\sim$1 cm^{-1}, the peak position stability in our experiments is much better than 1 cm^{-1} as observed experimentally, and therefore we believe that the peak shifts below 1 cm^{-1}, when comparing suspended and nonsuspended segments, are due to environmental effects.

Results and Discussion

To clarify any possible laser heating effect, we first collect Raman spectra for each SWNT at every point and compare its spectra using various laser power levels. For the SOS parts of almost all the nanotubes, there was no observable heating effect when using a laser power of $\leq$1.07 mW, which is consistent with what has been previously reported[15−17] and can be ascribed to the underlying substrate (SiO_2) as an effective heat sink.[18] However, for the SUS segments, the Raman spectra of most SWNTs show variations in RBM peak frequency, fwhm, and I_{AS}/I_S when changing the laser power from lower power levels to 1.07 mW (the highest power level in our setup), which indicates a heating effect for suspended SWNTs with a laser power of 1.07 mW. This can be explained by the poor thermal dissipation of the suspended SWNT to its surroundings due to its nanometer-scale cross section.[19,20] So to investigate the intrinsic Raman spectral variation for each SWNT, we first collect Raman spectra with different laser power levels for its SUS and SOS segments separately and make sure that the spectra we used for the discussion of the environmental effect below are free of laser heating.

Figure 2 shows Raman spectra obtained from the SUS and SOS segments of the same SWNT demonstrating the striking contrast between the spectra from the two segments. From our observations, the spectra from the SUS and SOS segments of the same SWNT may exhibit differences in intensity, frequency, fwhm, and I_{AS}/I_S for the RBM, and also differences in intensity, frequency, line shape, and fwhm for the various features of the G-band.

First of all, suspended SWNTs usually show enhanced Raman signals, which can be seen in Figure 2 as an example. This intensity-enhancement has been reported[17] previously and was attributed to an undisturbed environment for the suspended SWNTs. The enhanced signals are quite beneficial for both studying Raman features that are normally weak (such as the Raman peak at $\sim$1730 cm^{-1} in Figure 2) and enabling observation of SWNTs with a relatively poor resonance condition. In fact, for more than one-third of the SWNTs showing RBM Raman signals for the SUS segments, the corresponding SOS segments display no signals. According to our observations, the RBM intensity ratio of the Stokes signal obtained from the SUS segments to that obtained from the SOS segments (I_{SUS}/I_{SOS}) varies from one nanotube to another and a ratio of over 20 has been observed for particular tubes (see Table 1). Although most of the SWNTs show enhanced signals from their SUS segments compared with their SOS segments, there are also a few exceptions. Among the 15 SWNTs, there are two nanotubes (Nos. 6 and 9) with an RBM intensity ratio close to 1 and two other nanotubes (Nos. 2 and 4) with an RBM intensity ratio less than 1.

Although the SUS segments are expected to have an intrinsically higher Raman cross section[21] than the SOS segment, the electronic transition energies are also expected to change for the SUS segments relative to the SOS segments,[8,22] which can explain the smaller RBM intensity in the SUS segments as compared to the SOS segments in terms of the change in the resonance condition.

The RBM frequencies (ω_{RBM}) from the SUS and SOS segments of the same SWNT exhibit a small but observable shift in a few SWNTs. For an example, SWNT No. 6 shows an 0.9 cm^{-1} shift in the RBM frequencies. To see the spatial variation of ω_{RBM} and to ensure the repeatability of ω_{RBM} measurements, we have collected a series of spectra by moving the laser spot along the SWNT No. 6 from one side to the other side of the trench (6 μm wide, 10 μm deep) at 0.5 μm steps, and we have plotted its ω_{RBM} versus laser spot locations (see Figure 3). A clear difference in ω_{RBM} between the SUS and SOS segments is seen in Figure 3. Since the heating effect has been excluded, the difference must be due to the environmental variations along the nanotube. A possible explanation is the van der Waals interaction between the substrate and the SWNT. A previous work[9] has reported an ω_{RBM} shift for SWNT bundles under different pressures and has attributed this shift to the intertube van der Waals interactions.

The fwhms of the RBM are reduced significantly in the SUS segments compared with the SOS segments for about half of the SWNTs listed in Table 1, while a few SWNTs actually exhibit larger fwhm values in the SUS segments. We expect that the perturbation-free environment for the SUS segments will give rise to smaller fwhm in the SUS segments in general.[17] However, the change in the E_{ii} can affect the resonance condition $|E_{laser} - E_{ii}|$ and might increase the fwhm values in the SUS segments.[23]

The observed I_{AS}/I_S changes can be explained by the changes in E_{ii} values and the inverse lifetime of the intermediate electronic state. I_{AS}/I_S is given by the following:[2]

$$\frac{I_{AS}}{I_S}(\text{exp.}) = \frac{|(E_{laser} - E_{ii} - i\Gamma)(E_{laser} + E_{ph} - E_{ii} - i\Gamma)|^2}{|(E_{laser} - E_{ii} - i\Gamma)(E_{laser} - E_{ph} - E_{ii} - i\Gamma)|^2} \exp\left(-\frac{E_{ph}}{k_B T}\right) \quad (1)$$

where E_{laser} and E_{ii} have the same meaning as formerly defined, E_{ph} is the phonon energy (ω_{RBM}), Γ is the inverse lifetime of the intermediate electronic state, k_B is the Boltzmann constant, and T is the temperature of the SWNT. As the laser heating is excluded, the I_{AS}/I_S variation between the SUS and SOS segments of a SWNT must come from either E_{ii} or Γ variations. Although our instrument does not have the capability to measure E_{ii} and Γ values, our results indicate that there is significant E_{ii} variation, at least for a few SWNTs. For example, the No. 10 nanotube has a thermal factor of $\exp(-E_{ph}/k_BT) = 0.47$ at room temperature ($T = 298$ K), and its I_{AS}/I_S values are 0.96 and 0.39 for the SUS and SOS segments, respectively. This indicates that $E_{ii} > E_{laser}$ for the SUS segment and $E_{ii} < E_{laser}$ for the SOS segment for this nanotube. With a similar argument, we can conclude that the E_{ii} of nanotube No. 13 also downshifts in the SOS segment, whereas it is highly possible that the E_{ii} of nanotube No. 14 upshifts in the SOS segment. If E_{ii} of nanotube No. 14 did not shift at all, or if it downshifted, the Γ value must be significantly smaller in the SOS segment than in the SUS segment, which contradicts the assumption that the SUS segment is free of environmental perturbation and should have a longer lifetime of the intermediate electronic state.

There are several possible explanations for the E_{ii} variations. The first one is the charge transfer between the substrate and the SWNT. However, this is not very likely in our samples since the SiO_2 is an insulating material. Another possible explanation is the different dielectric environment giving rise to the difference in the electron−electron Coulomb repulsion and the exciton binding energies.[24,25] This is also excluded since this effect is weakly sensitive to the SWNT chirality[26] and would shift the E_{ii} in the same direction for all the SWNTs, which is not consistent with our experimental results. The last explanation is in terms of the van der Waals interaction between the substrate and the SWNT. Theoretical calculations showed that for nanotubes on a flat metal surface, the binding energy between the substrate and the SWNT will introduce a radial deformation and alter its electronic properties.[27,28] It is also expected that the van der Waals interactions between a SWNT and a silicon substrate distort the cross section of nanotubes and that the distorted tube cross-section leads to a change in its electronic properties.[6]

The radial deformation induced by the nanotube−substrate interaction will most likely result in strain in the radial direction in the nanotube. And on the other hand, the E_{ii} of semiconducting nanotubes was reported to shift in two directions depending on their $(2n+m)$ mod 3 = 1 or 2 family type.[5,29,30] We make tentative (n,m) assignments for these three nanotubes using a previously reported method.[3,13] Nanotube No. 13 can be assigned to one of following nanotubes—(24,1)/(18,10)/(19,8)/(23,3)—which all fall into an $(2n+m)$ mod 3 = 1 family (type I), and the laser excitation energy used in this experiment corresponds to an E_{44} transition for this nanotube. Nanotube No. 14 is one of (25,3)/(23,7)/(20,10), which all fall into the $(2n+m)$ mod 3 = 2 family (type II), and the observed optical transition corresponds to an E_{44} transition. Similarly, tube No. 10 belongs to the $(2n+m)$ mod 3 = 2 family (type II) and the optical transition corresponds to an E_{33} transition. The analysis given above showed that the E_{ii} of nanotubes No. 10 and No. 13 downshifts and the E_{ii} of nanotube No. 14 upshifts in SOS segments compared to SUS segments. This is consistent with the predicted family behavior of E_{ii} shifting for SWNTs under strain. Note that for nanotubes with the same type, its E_{33} and E_{44} should shift in reverse direction under strain.

The G-band of semiconducting SWNTs show little change except for a couple of SWNTs that exhibit a small shift of about 5 cm^{-1} in the G^--mode frequency (see Figure 4b). The SWNT in Figure 4b did not show an RBM signal in the SOS segment and therefore is not included in Table 1. The G^--mode frequency is related to the curvature of the SWNT wall.[31] This is consistent with a possible radial deformation due to the van der Waals interaction between the substrate and the SWNT, although it still remains unclear why the RBM frequency variation often does not coincide with the G^--mode frequency variation.

On the other hand, the G-band of a few metallic SWNTs shows a striking difference between the SUS and SOS segments (see Figures 4a). First of all, the relative intensity between the higher frequency peak and the lower frequency Breit−Wigner−Fano (BWF) peak changes dramatically. Second, the frequency of the BWF peak or higher frequency peak often shifts, although the shift directions vary for different SWNTs. We believe that these changes are due to the electronic band structure modulation since the metallic G-band shape and frequency are closely related to the electron−phonon interaction and by changing the electronic band structure the strength of this interaction would change.[31−37] Unfortunately, at present there is no single theoretical model that can explain every detail of the observations we have made on these samples.

Conclusions

We prepared partially suspended individual long SWNTs on trench-contained substrates and carried out a systematic inves-

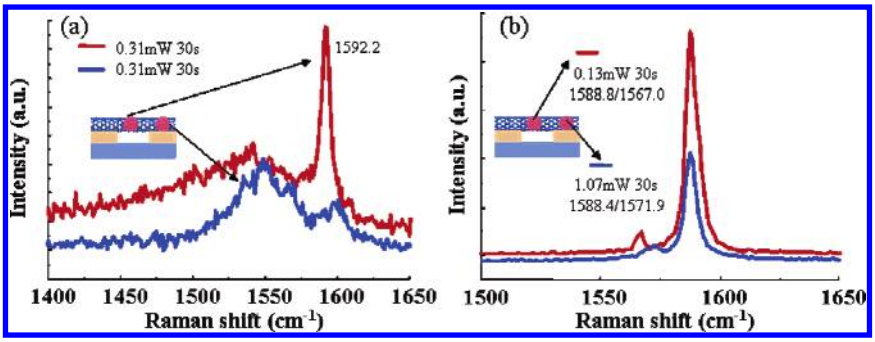

Figure 4. G-mode Raman spectra of two individual SWNTs (a and b) taken from suspended segments and from segments sitting on substrate. The laser power level, the integration time, and the corresponding peak positions (in cm^{-1}) are shown in the inset. The peak positions in part a cannot be determined well due to its complicated line shape.

tigation of the difference between SUS and SOS segments of 15 individual SWNTs. With the heating effect being excluded by using low laser power, spectral differences between the SUS and SOS segments of the same nanotube are recorded and analyzed. Most of the SWNTs under investigation show enhanced Raman signals at their SUS segment compared with the SOS ones, with the exceptions that two of the tubes exhibit a similar Raman intensity at the SUS and SOS locations and two tubes show a reverse result. Along with the distinct intensity contrast, moderate RBM frequency variations are observed for some nanotubes, and these variations can be attributed to nanotube−substrate interaction. By analyzing the behaviors of the fwhm and I_{AS}/I_S of RBM, we find out that the E_{ii} of SWNTs shift when comparing the two different types of segments. Considering all possible reasons for the E_{ii} variation, we believe that for our system the main reason is van der Waals interactions between the SWNT and the substrate, which may deform the SWNT sitting on the substrate in the radial direction and thereby modify its electronic DOS, while suspended nanotubes still retain their pristine properties. Although the very detailed mechanisms behind these spectral differences are not very clear yet, our work provides evidence for the local property tuning of individual SWNTs by environmental effects. The approach taken in the present study can be readily extended to other 1D materials and can lead to a facile way to generate and manipulate diverse properties of a single 1D object.

Acknowledgment. This work was supported by NSFC (20573002, 20673004, 50521201), MOST (2006CB0N0701, 2006CB0N0403), and the FOKYING TUNG Education Foundation (94012). H.S. and J.K. gratefully acknowledge support from the Intel Higher Education Program. M.S.D. acknowledges support from NSF DMR 04-05538.

References and Notes

(1) Dresselhaus, M. S.; Dresselhaus, G.; Saito, R.; Jorio, A. *Phys. Rep.* **2005**, *409*, 47.

(2) Fantini, C.; Jorio, A.; Souza, M.; Strano, M. S.; Dresselhaus, M. S.; Pimenta, M. A. *Phys. Rev. Lett.* **2004**, *93*, 147406.

(3) Jorio, A.; Saito, R.; Hafner, J. H.; Lieber, C. M.; Hunter, M.; McClure, T.; Dresselhaus, G.; Dresselhaus, M. S. *Phys. Rev. Lett.* **2001**, *86*, 1118.

(4) Ericson, L. M.; Pehrsson, P. E. *J. Phys. Chem. B* **2005**, *109*, 20276.

(5) Yang, L.; Han, J. *Phys. Rev. Lett.* **2000**, *85*, 154.

(6) Hertel, T.; Walkup, R. E.; Avouris, P. *Phys. Rev. B* **1998**, *58*, 13870.

(7) Maiti, A. *Nat. Mater.* **2003**, *2*, 440.

(8) Petrov, A. G.; Rotkin, S. V. *Nano Lett.* **2003**, *3*, 701.

(9) Venkateswaran, U. D.; Rao, A. M.; Richter, E.; Menon, M.; Rinzler, A.; Smalley, R. E.; Eklund, P. C. *Phys. Rev. B* **1999**, *59*, 10928.

(10) Alvarez, L.; Righi, A.; Guillard, T.; Rols, S.; Anglaret, E.; Laplaze, D.; Sauvajol, J. L. *Chem. Phys. Lett.* **2000**, *316*, 186.

(11) Henrard, L.; Hernandez, E.; Bernier, P.; Rubio, A. *Phys. Rev. B* **1999**, *60*, R8521.

(12) Rao, A. M.; Chen, J.; Richter, E.; Schlecht, U.; Eklund, P. C.; Haddon, R. C.; Venkateswaran, U. D.; Kwon, Y. K.; Tomanek, D. *Phys. Rev. Lett.* **2001**, *86*, 3895.

(13) Zhang, Y. Y.; Zhang, J.; Son, H. B.; Kong, J.; Liu, Z. F. *J. Am. Chem. Soc.* **2005**, *127*, 17156.

(14) Zheng, L. X.; O'Connell, M. J.; Doorn, S. K.; Liao, X. Z.; Zhao, Y. H.; Akhadov, E. A.; Hoffbauer, M. A.; Roop, B. J.; Jia, Q. X.; Dye, R. C.; Peterson, D. E.; Huang, S. M.; Liu, J.; Zhu, Y. T. *Nat. Mater.* **2004**, *3*, 673.

(15) Dresselhaus, M. S.; Dresselhaus, G.; Jorio, A.; Souza, A. G.; Saito, R. *Carbon* **2002**, *40*, 2043.

(16) Souza, A. G.; Chou, S. G.; Samsonidze, G. G.; Dresselhaus, G.; Dresselhaus, M. S.; An, L.; Liu, J.; Swan, A. K.; Unlu, M. S.; Goldberg, B. B.; Jorio, A.; Gruneis, A.; Saito, R. *Phys. Rev. B* **2004**, *69*, 115428.

(17) Son, H. B.; Hori, Y.; Chou, S. G.; Nezich, D.; Samsonidze, G. G.; Dresselhaus, G.; Dresselhaus, M. S.; Barros, E. B. *Appl. Phys. Lett.* **2004**, *85*, 4744.

(18) Pop, E.; Mann, D.; Cao, J.; Wang, Q.; Goodson, K.; Dai, H. J. *Phys. Rev. Lett.* **2005**, *95*, 155505.

(19) Itkis, M. E.; Borondics, F.; Yu, A. P.; Haddon, R. C. *Science* **2006**, *312*, 413.

(20) Cao, H.; Wang, Q.; Wang, D. W.; Dai, H. J. *Small* **2005**, *1*, 138.

(21) Corio, P.; Santos, P. S.; Pimenta, M. A.; Dresselhaus, M. S. *Chem. Phys. Lett.* **2002**, *360*, 557.

(22) Maiti, A.; Ricca, A. *Chem. Phys. Lett.* **2004**, *395*, 7.

(23) Reich, S.; Thomsen, C.; Ordejon, P. *Phys. Rev. B* **2002**, *65*, 155411.

(24) Ando, T. *J. Phys. Soc. Jpn.* **1997**, *66*, 1066.

(25) Perebeinos, V.; Tersoff, J.; Avouris, P. *Phys. Rev. Lett.* **2004**, *92*, 257402.

(26) Samsonidze, G. G.; Saito, R.; Kobayashi, N.; Gruneis, A.; Jiang, J.; Jorio, A.; Chou, S. G.; Dresselhaus, G.; Dresselhaus, M. S. *Appl. Phys. Lett.* **2004**, *85*, 5703.

(27) Dag, S.; Gulseren, O.; Ciraci, S.; Yildirim, T. *Appl. Phys. Lett.* **2003**, *83*, 3180.

(28) Park, N.; Hong, S. *Phys. Rev. B* **2005**, *72*, 045408.

(29) Karaiskaj, D.; Engtrakul, C.; McDonald, T.; Heben, M. J.; Mascarenhas, A. *Phys. Rev. Lett.* **2006**, *96*, 106805.

(30) Souza, A. G.; Kobayashi, N.; Jiang, J.; Gruneis, A.; Saito, R.; Cronin, S. B.; Mendes, J.; Samsonidze, G. G.; Dresselhaus, G. G.; Dresselhaus, M. S. *Phys. Rev. Lett.* **2005**, *95*, 217403.

(31) Jorio, A.; Pimenta, M. A.; Souza, A. G.; Saito, R.; Dresselhaus, G.; Dresselhaus, M. S. *New J. Phys.* **2003**, *5*, 139.

(32) Popov, V. N.; Lambin, P. *Phys. Rev. B* **2006**, *73*, 085407.

(33) Lazzeri, M.; Piscanec, S.; Mauri, F.; Ferrari, A. C.; Robertson, J. *Phys. Rev. B* **2006**, *73*, 155426.

(34) Bose, S. M.; Gayen, S.; Behera, S. N. *Phys. Rev. B* **2005**, *72*, 153402.

(35) Jiang, C. Y.; Kempa, K.; Zhao, J. L.; Schlecht, U.; Kolb, U.; Basche, T.; Burghard, M.; Mews, A. *Phys. Rev. B* **2002**, *66*, 161404.

(36) Brown, S. D. M.; Jorio, A.; Corio, P.; Dresselhaus, M. S.; Dresselhaus, G.; Saito, R.; Kneipp, K. *Phys. Rev. B* **2001**, *6315*, 155414.

(37) Shim, M.; Ozel, T.; Gaur, A.; Wang, C. J. *J. Am. Chem. Soc.* **2006**, *128*, 7522.